Dynamic Behaviour of Railway Ballasted Track Structures in Shaking Table Tests and Seismic Resistant Performance Evaluation in Japan

T. Ishikawa[1], S. Miura[2] and E. Sekine[3]
[1,2]*Faculty of Engineering, Hokkaido University, Sapporo, Japan*
[3]*Hokubu Consultant Co. LTD., Tokyo, Japan*
[1]*E-mail:* t-ishika@eng.hokudai.ac.jp

ABSTRACT: This study presents an experimental, analytical and numerical studies to elucidate the dynamic response of ballasted track structures subjected to horizontal seismic motions. First, a series of shaking table tests for one-third small-scale model ballasted tracks was performed. As the results, it was revealed that the existence of grouted layer had a serious influence on the seismic performance of ballasted track structures. Next, numerical simulations of the shaking table tests were conducted with a newly proposed analytical procedure which utilizes FE analysis considering the cumulative strain characteristics of ballast. As the results, it was revealed that as the analytical procedure could roughly estimate the residual displacement of railroad ballast after seismic motions, it was effective to evaluate the seismic performance of ballasted track structures for practical use.

1. INTRODUCTION

After the 1995 Hyougoken-Nambu Earthquake, a two-stage seismic design procedure to investigate the aseismic performance of structures under a strong seismic motion (Level 2 seismic motion), which has a low probability of occurrence during the designed useful life of the structures, and under conventionally considered seismic motion with high probability of occurrence (Level 1 seismic motion), was proposed by the Japan Society of Civil Engineers (JSCE). This new seismic design procedure is a calculation method to check whether the damage and deformation of civil structures resulting from an earthquake including Level 2 seismic motion satisfy the designed aseismic performance. In accordance with this proposal, a new standard "Design standard for Railway Structures - Seismic Design - (RTRI, 1999)" was newly adopted by the Ministry of Land, Infrastructure, Transport and Tourism in 2008. However, track structures such as ballasted track and slab track are excluded from the target of the new design standard, though track structures considerably affect the running safety and riding comfort for operated trains.

In Japan, buckling of track skeleton and severe track irregularity caused by plastic flow of railroad ballast and/or deterioration in lateral resistance of railroad ballast resulting from strong seismic motion have been reported by past researches (e.g. Suda et al., 1997). The buckling and track irregularity lead to deterioration in the running safety of railway operation, even on ballasted tracks without remarkable deformation in other structures (Miura and Kirishiki, 1982; Miura, 1996). Therefore, it is necessary to establish a method for evaluating the aseismic performance of ballasted track structures, and the method should involve the usage of dynamic response analysis for predicting the plastic flow and/or deterioration in lateral resistance of railroad ballast caused by an earthquake.

However, so far no dynamic response analysis which can examine the above-mentioned phenomena related to its ductility has been utilized for aseismic performance assessment in Japan, while static analysis for evaluating seismic stability expected in the track structures when an inertia force due to earthquake acts, namely "Seismic coefficient method", has been conventionally conducted. The reason for this is that many unsolved subjects concerning dynamic properties of ballasted track structures remain compared with other railway structures, although ballasted track as shown in Figure 1 accounts for nearly 80 % of Japanese railway track. Here, CAM stands for cement asphalt mortar. Above all, there are few studies to examine the seismic stability and ductility of ballasted track in intense earthquake because non-linear behavior of "railroad ballast," a component of ballasted track consisted of coarse granular materials, is much complicated. Therefore, at present, the development of a new seismic design standard for track structures adopting the two-stage seismic design procedure needs to establish a method for assessing the aseismic performance of ballasted track structures with the dynamic response analysis, which is prescribed by the design standard for railway structures, with consideration given to the ductility against Level 2 seismic motion.

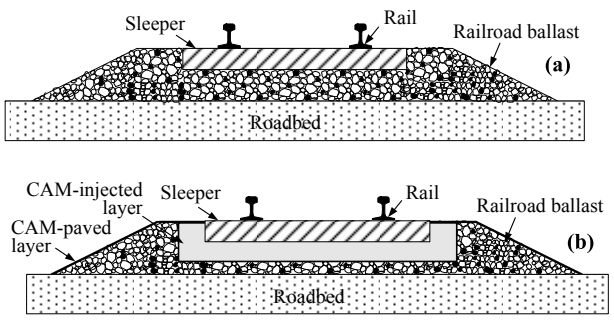

Figure 1 Ballasted track structure (cross-section, a: conventional ballasted track, b: grouted ballasted track)

This paper presents an experimental, analytical and numerical study to elucidate the dynamic response of railroad ballast subjected to strong horizontal vibrations and to propose a simple and practical seismic calculation method for evaluating the aseismic performance of ballasted track structures under Level 2 seismic motion. For this purpose, first a series of shaking table tests for two types of small-scale model ballasted tracks, namely conventional ballasted track (Figure 1a) and grouted ballasted track (Figure 1b) was performed under cyclic sinusoidal-waves with a variety of loading frequencies and acceleration amplitudes. Here, grouted ballasted track is a kind of maintenance-free track structures characterized by paved tracks in which railroad ballast is partially solidified by asphalt-mixture materials. Based on the test results, the seismic stability and ductility beyond failure of railroad ballast are qualitatively and quantitatively evaluated associated with the observed movement of ballast particles inside railroad ballast during seismic motion. Next, we introduce a new analytical procedure which utilizes iterative calculation with Finite Element (FE) analysis to estimate cyclic plastic deformation of ballasted track under seismic loads in terms of the deformation-strength characteristics of railroad ballast. For the simplicity of numerical model, instead of the introduction of cyclic plastic constitutive models, the analytical procedure reproduce cyclic plastic deformation of railroad ballast suffered from seismic loads by considering the cumulative strain characteristics, which were estimated based on the results of cyclic triaxial compression tests. In this study, numerical simulations of the above-mentioned shaking table tests were conducted to evaluate the applicability and usefulness of the proposed analytical procedure.

From the comparison of experimental results with the numerical simulations, we discuss the validity and the applicability of the proposed analytical procedure in predicting the residual displacement of railroad ballast after seismic motions.

2. SHAKING TABLE TESTS

2.1 Testing methods

2.1.1 Ballast samples

In Japan, railroad ballast is usually composed of uniformly graded crushed andesite stone, namely "ballast". Figure 2 shows the grain size distribution curve for ballast (hereafter, "1/1 ballast") employed in the actual railway track and model ballast (hereafter, "1/3 ballast") used in this study, together with its mean grain sizes (D_{50}) and uniformity coefficients (U_c). Note that dotted lines shows the proper grading limits of railroad ballast provided by the Japanese railway specification. Accordingly, as shown in Figure 2, test sample (1/3 ballast) in this study has one-third mean grain size distribution of actual ballast and the grain size distribution similar to that of 1/1 ballast. In this connection, Ishikawa and Sekine (2003) revealed the validity of one-third scale model using 1/3 ballast in shaking table tests in terms of deformation and damage of railroad ballast compared with the seismic performance of full scale model using 1/1 ballast.

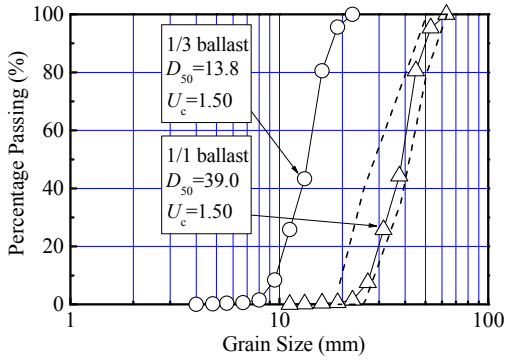

Figure 2 Grain size distribution of ballast sample

2.1.2 Test implements

The general arrangement of shaking table tests for one-third scale models of a full-scale track employed normally in Japanese railway is shown in Figure 3. The model track, which simulates a transverse section of real ballasted track, is in the plane strain state assuming the transverse section to be infinitely continued. Here, the discontinuity of the sleepers in the longitudinal direction is not considered, as it is conducted under plane strain condition as in the case of two-dimensional FE analysis. This study therefore used continuous model sleepers for the direction of depth. To ensure the model in the plane strain state, a lubrication layer composed of silicone grease and a transparent vinyl film was inserted between the side walls of soil container and model track. In this study, the term "B-track" are used to refer to the conventional ballasted track, and the term "G-track" are used to refer to the grouted ballasted track. In this study, we assume the following grouted track that there are no paved layers at the shoulders and slope faces of railroad ballast.

The ballasted track was composed of railroad ballast, concrete sleeper, and steel roadbed (Note that there is no rail though weights corresponding to self-weight of rail per unit length are put on the position). The railroad ballast was moulded into the form similar to the transverse section of the real ballasted track by tamping with a wooden rammer. The initial dry density (ρ_d) of railroad ballast was set to ρ_d=1.60g/cm^3, by referring to actual dry density measured at ballasted track (Sunaga et al., 1995). The railroad ballast was kept air-dried condition throughout the test. As for roadbed, to increase the surface-roughness between railroad ballast and roadbed, the surface was covered by cement asphalt mortar (CAM) and the small gravels of 2 mm in diameter were glued on the surface. In addition to ballasted track, grouted track has a CAM-injected layer around a concrete sleeper, in which single-grained gravel of 4.0 - 6.7 mm and CAM are mixed. Figure 4 shows a result of unconfined compression test on CAM.

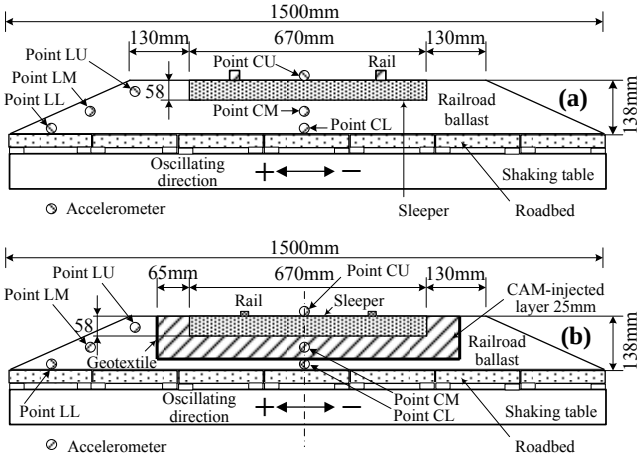

Figure 3 Shaking table test of model ballasted track (a: conventional ballasted track, b: grouted ballasted track)

To measure the dynamic response of railroad ballast, displacement transducers and accelerometers were installed to the model track as shown in Figure 3. Throughout shaking table tests, the horizontal input base acceleration and displacement of a shaking table, the horizontal response acceleration of a sleeper, railroad ballast, and roadbed, and the horizontal and vertical response displacement of a sleeper were simultaneously recorded at the sampling frequency of 400 Hz and stored by a computer. Besides, to observe the deformation of railroad ballast under shaking, a number of targets, that is white-coloured ballast particles, were placed adjacent to the front transparent side wall. The movements of the targets were recorded at all test stages by using a high-speed CCD (charge-coupled device) camera (frame rate: 200 fps, resolution: 512 ×512 pixels), and after tests, they were traced by analysing the photographs of model track. The sign of horizontal acceleration and horizontal displacement were defined as shown in Figure 3.

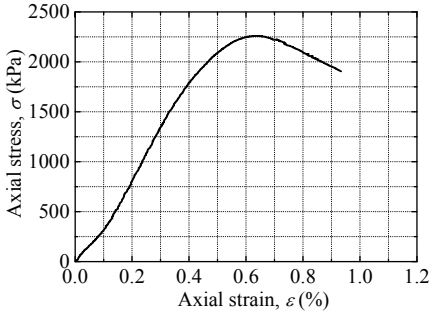

Figure 4 Result of unconfined compression test on CAM

2.1.3 Test procedure

Seismic loads were applied by shaking the soil container horizontally with a sinusoidal base acceleration. Each specimen was subjected to several shaking steps, where the input single amplitude of base acceleration ($a_{i,sa}$) was initially set to 1.0 m/s^2 and increased at an increment of 1.0 m/s^2 after every 10 cycles as shown in Figure 5. Shaking was terminated when the base acceleration had reached the allowable maximum amplitude in terms of hardware constraints. The loading frequency (f) is fixed at 5 Hz. The step-loading method in this study was set by referring to "Method for Cyclic Triaxial Test to Determine Deformation Properties of Geomaterials (JGS 0542-2000)".

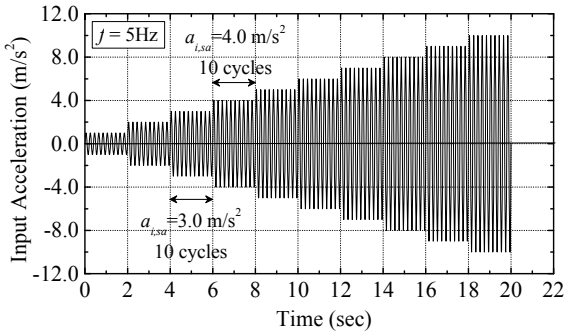

Figure 5 Horizontal input motions in shaking table test

Since sinusoidal waves with constant amplitude can hardly simulate actual seismic waves, this study targets the basic examination on the dynamic deformation properties of ballasted tracks like JGS 0542. Table 1 shows experimental conditions of all tests. Moreover, sweep tests were performed to examine resonant frequency of the shaking table - model track systems. The base acceleration in sweep tests was given by sinusoidal waves of f=1-10Hz and $a_{i,sa}$=0.5m/s^2. Figure 6 shows the relation of both model tracks between the amplification factor of acceleration at the center of upper sleeper surface and the loading frequency of the input base acceleration. The term "amplification factor" can be defined as the ratio of the maximum response to the single amplitude of input waves. As it is clear from Figure 6, both model tracks have no clear resonant frequencies in the range of 1 - 10 Hz.

Table 1 Experimental conditions of shaking table tests

Loading frequency	Input single amplitude of base acceleration	Input single amplitude of base displacement
5 Hz	2.0 m/s^2	10 mm
5 Hz	4.0 m/s^2	20 mm
5 Hz	6.0 m/s^2	30 mm
5 Hz	8.0 m/s^2	40 mm
5 Hz	10.0 m/s^2	50 mm

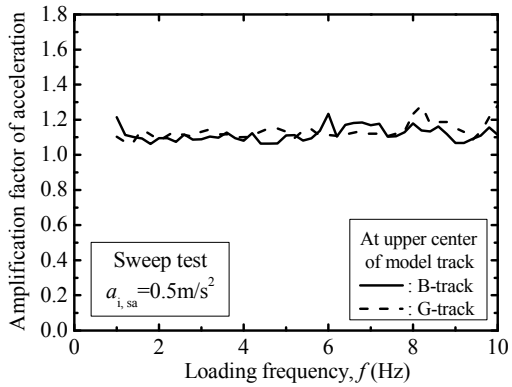

Figure 6 Frequency response of model ballasted track

2.2 Results and discussions

2.2.1 Difference in Time history response

The influence of experimental conditions on the dynamic behavior of model tracks under horizontal vibrations is discussed. Figure 7 shows typical time histories of horizontal response displacement (u) at Point CU of B-track in Figure 3 under various vibration conditions ($a_{i,sa}$=2.0, 8.0m/s^2 while f=5Hz). Here, the horizontal response displacement is defined as the horizontal movement of a target on the sleeper, which can be calculated by analyzing photographs taken during shaking.

From Figure 7, it is recognized that the amplitude of response displacement increases with the input single amplitude of base acceleration ($a_{i,sa}$). Furthermore, the response displacement after shaking does not return to zero in the case of high $a_{i,sa}$ equal to 8.0 m/s^2, while the displacement is almost zero in case of $a_{i,sa}$=2.0m/s^2. Then, the horizontal residual displacement (u_p) for any desired target can be defined as the difference in the horizontal coordinate before and after shaking. It can be observed in Figure 7 that horizontal residual displacement increases with the input base acceleration. Therefore, the dynamic behavior of railroad ballast tends to gradually change from quasi-elastic response to plastic response with the increase in $a_{i,sa}$. On the other hand, comparing time history responses of B-track with these of G-track, the difference in dynamic behavior of model tracks is hardly observed in case of $a_{i,sa}$=2.0m/s^2, while at $a_{i,sa}$=8.0m/s^2 the amplitude of response displacement and the magnitude of residual displacement in G-track are much smaller than those in B-track. These phenomena seem to be caused by the plastic flow of railroad ballast subjected to strong seismic motion.

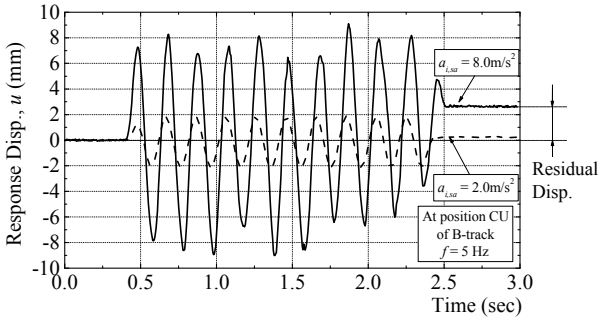

Figure 7 Time histories of response displacement in B-track

2.2.2 Dynamic response characteristics of railroad ballast

The influence of vibration conditions on the dynamic response properties of railroad ballast to horizontal input base motions is discussed by comparing test results of B-track with those of G-track. Figure 8 compares the amplification factor of acceleration and the normalized height at various measuring positions along the left end slope and the center line of railroad ballast (positions LU, LM, LL, CU, CM and CL in Figure 3) in B-track and G-track obtained from shaking table tests under $a_{i,sa}$=2.0, 8.0m/s^2. Here, the normalized height is calculated as the ratio of vertical length from upper surface of the shaking table to the accelerometer position against the height of model track. Figure 9 shows the relationships between the amplification factor of acceleration and the input single amplitude of base acceleration ($a_{i,sa}$) at the upper center of model sleeper (position CU in Figure 3) in both ballasted tracks.

In Figure 8, as for B-track, the difference in the amplification factor of acceleration owing to the measuring position cannot be distinguished at $a_{i,sa}$=2.0m/s^2, while the amplification factor of acceleration at $a_{i,sa}$=8.0m/s^2 is larger than that at $a_{i,sa}$=2.0m/s^2 when comparing under the same position, and the increasing tendency becomes more remarkable with the location of accelerometer going upward, irrespective of the horizontal location in railroad ballast. These results indicate that when the effect of the inertia of a sleeper on the dynamic behavior of ballasted track structures becomes strong with input base acceleration increase, the dynamic interaction between a sleeper and railroad ballast comes up to the surface, thereby exerting the conspicuous influence on the coseismic behavior of B-track. On the other hand, as for the G-track, the amplification factor of acceleration remains nearly constant at the center of railroad ballast regardless of input base acceleration, while it increases with increasing $a_{i,sa}$ at the left end of railroad ballast, and the increasing tendency is obviously seen in the upper layer of railroad ballast. The reason for this seems to be that the existence of grouted layer seriously loses a distinctive feature of railroad ballast as a granular material, and as the result a sleeper, railroad ballast, and roadbed vibrate together in one piece with little phase difference.

Accordingly, these results lead to the conclusion that the mobility of individual ballast particles under horizontal vibrations has a significant influence on the dynamic response of ballasted track structures.

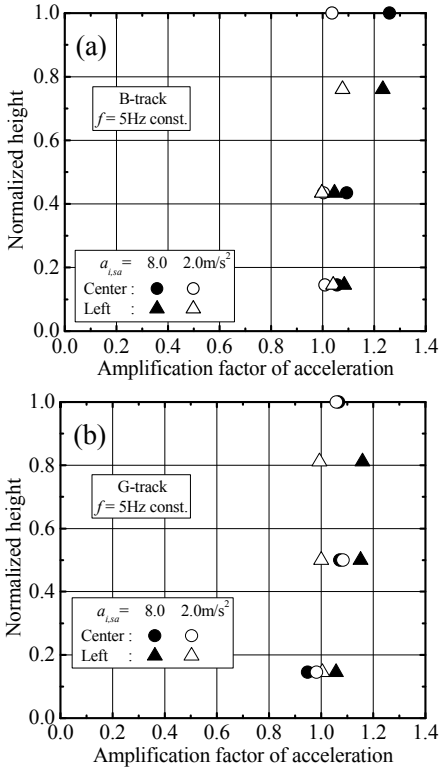

Figure 8 Distribution of amplification factor of acceleration (a: conventional ballasted track, b: grouted ballasted track)

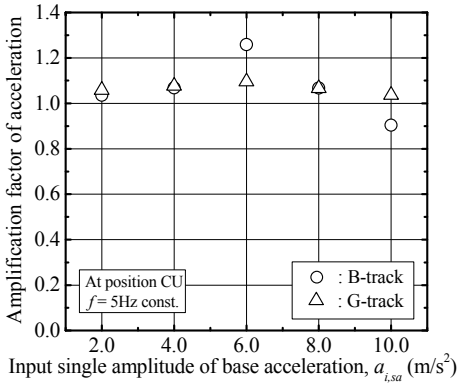

Figure 9 Dependency of response acceleration on input frequency

In Figure 9, as for B-track, the amplification factor of acceleration increases with increasing $a_{i,sa}$ at the range of small $a_{i,sa}$, while it dramatically decreases after $a_{i,sa}$ exceeds 6.0 m/s^2. This phenomenon seems to be related to the change in the dynamic response behavior of railroad ballast, caused by strong vibrations, from elastic deformation to plastic deformation. The reason for this can be considered to be that though the decrease in the stiffness of railroad ballast due to cyclic horizontal vibrations leads to the gentle increase in the amplification factor of acceleration at the range of $a_{i,sa}$=6.0m/s^2 or less, over $a_{i,sa}$=6.0m/s^2 where the generation of local plastic flow inside railroad ballast becomes remarkable, the interlocking between ballast particles and/or between a sleeper and ballast particles deteriorates, thereby causing insufficient transmission of exciting force. On the other hand, as for G-track where the residual displacement after horizontal vibrations is hardly observed at the railroad ballast even if $a_{i,sa}$ is high, the amplification factor of acceleration remains nearly constant regardless of $a_{i,sa}$. These indicate that the response acceleration characteristics for ballasted track structures have high correlation to a tendency for the dynamic response behavior of railroad ballast to become plastic.

2.2.3 Damage of railroad ballast

In a two-stage seismic design procedure of earth structures, the allowable damage in the case of Level 2 seismic motion differs from that for Level 1 seismic motion. For Level 1 seismic motion, the objective of seismic design is that the original functions of structures should not deteriorate, maintaining the original design requirement after the earthquake. Whereas, for Level 2 seismic motion, the objective is to ensure that the damage should not seriously affect the original functions of the structure and adjacent facilities even if some degree of damage occurs. Therefore, in this section, the seismic stability and ductility of ballasted track structures beyond failure are discussed.

Figure 10 compares the relationships between the residual displacement (u_p) and the normalized height at various measuring positions along the left end slope and the center line of railroad ballast (positions LU, LM, LL, CU, CM and CL in Figure 3) in B-track and G-track obtained from the shaking table tests under $a_{i,sa}$=2.0, 8.0m/s^2. As for B-track, residual displacement is hardly observed at any positions of railroad ballast in the case of $a_{i,sa}$=2.0m/s^2, while once the dynamic behavior of railroad ballast becomes plastic as $a_{i,sa}$ increase to 8.0 m/s^2, the magnitude of horizontal residual displacement varies significantly depending on not only the vertical position but also the horizontal position. The residual displacement tends to increase with the location inside railroad ballast going upward and leftward. The reason for this seems to be that the confining pressure to each ballast particle decreases as its location goes away from the center of railroad ballast and/or toward upper layer of railroad ballast and as a consequence the mobility of individual ballast particles under horizontal vibrations increases. These results indicate that the evaluation of the seismic stability and ductility of coarse granular materials needs to estimate the mobility of constituent particles because a large movement of constituent particles causes local plastic flow in an overall granular body.

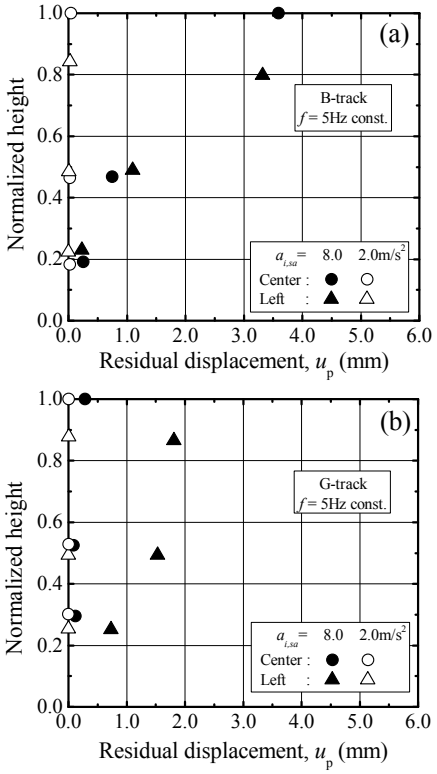

Figure 10 Distribution of residual displacement (a: conventional ballasted track, b: grouted ballasted track)

On the other hand, although a tendency similar to the above-mentioned can be observed at G-track, the residual displacement of G-track is smaller than that of B-track when compared under the same experimental conditions. Especially, even in case of $a_{i,sa}$=8.0 m/s^2, u_p hardly generates in the center part of G-track. Furthermore, the distribution of residual displacement caused by horizontal vibrations approximately corresponds to the increasing tendency of the amplification factor of acceleration. Accordingly, from these results, it seems reasonable to conclude that in case of the seismic design against Level 2 seismic motion, which needs the evaluation of the ductility of ballasted track structures beyond failure as well as the seismic stability, the grouted ballasted track exhibits higher aseismic performance than the conventional ballasted track because the former can restrain the damage of railroad ballast caused by seismic motions as compared with the latter.

These results revealed that the edges and the adjacent area of railroad ballast such as ballast shoulder and slope face was considered to be prone to damages due to seismic motion and exhibit the weakest aseismic performance among various components of ballasted track structures. Besides, as mentioned above, it has been shown that there is a high correlation between the plastic deformation of railroad ballast, and the decrease in the lateral resistance of railroad ballast or the occurrence of the severe track irregularity after an earthquake. Therefore, in this study, we examine the calculation method to predict the residual displacement of railroad ballast due to an earthquake by focusing on the cyclic plastic deformation characteristics of ballast as an indicator to evaluate the aseismic performance of ballasted track structures.

3. CUMULATIVE DAMAGE ANALYSIS

3.1 Cumulative strain characteristics of ballast

According to past researches, when an embankment comprised of sandy soils is subjected to seismic motions, its stiffness deteriorates depending on the cyclic shear strength and number of loading cycles, and this results in the accumulation of plastic axial strain. In addition, the relationship between the cyclic load and the cumulative axial strain is influenced by the initial shear stress inside the embankment. Therefore, in the "Design standard for Railway Structures - Seismic Design –", the cumulative axial strain ($(\varepsilon_a)_{max}$) is formulated by Horii et al. (1997) as shown in Eq. (1). Here, the initial shear stress ratio (SR_s), dynamic shear stress ratio (SR_d), and number of loading cycles (N_c) are input parameters, and coefficients $a1$ to $a7$ are determined from the results of the cyclic triaxial compression tests conducted by Hirano et al. (1997) on sandy soil materials. The definition of each stress is shown in Figure 11.

$$\left.\begin{aligned}(\varepsilon_a)_{max} &= \left(\frac{SR_d}{a1\cdot(a2-a3\cdot SR_s^{a4})\cdot N_c^{a5}}\right)^{a6\cdot N_c^{a7}} \\ SR_s &= \tau_s/\sigma_m = \sigma_s/(2\sigma_m), \quad SR_d = \tau_d/\sigma_m = \sigma_d/(2\sigma_m)\end{aligned}\right\} \quad (1)$$

Where, τ_s : initial shear stress; τ_d : cyclic shear stress amplitude; σ_m : mean principal stress; σ_s : initial deviator stress; σ_d : cyclic axial stress amplitude. In this study, we assume that the cumulative strain characteristics of ballast can be expressed in an equation similar to Eq. (1) for the cumulative strain characteristics of sandy soil materials. Accordingly, we elucidated the relationships between SR_s, SR_d, N_c, and $(\varepsilon_a)_{max}$ by determining the coefficients $a1$ to $a7$ in Eq. (1) from the results of the cyclic triaxial compression tests on 1/3 ballast (Figure 2) used in the shaking table model test for model tracks.

Figure 12 shows the relationship between the axial strain (ε_a) and N_c obtained from the cyclic triaxial compression tests (ρ_d=1.60 g/cm^3; effective confining pressure σ_c'=29.4kPa (isotropic consolidation); deviator stress amplitude q_a=100kPa (q_{max}=110kPa, q_{min}=10kPa); f=0.25Hz, Kohata et al., 2003). Note that ε_a shows the value measured by regarding an axial strain at Point A (in Figure 11) as the origin, and $(\varepsilon_a)_{max}$ indicates the axial strain when the maximum deviator stress (q_{max}) is applied during cyclic loading. From the figure, it is inferred that though the axial strain tends to increase with cyclic loading, the increase in the residual axial strain becomes smaller as N_c increases, and that the deformation behavior of ballast is elasto-plastic with higher plasticity during the initial stage of cyclic loading, while it shifts to elastic behavior with cyclic loading.

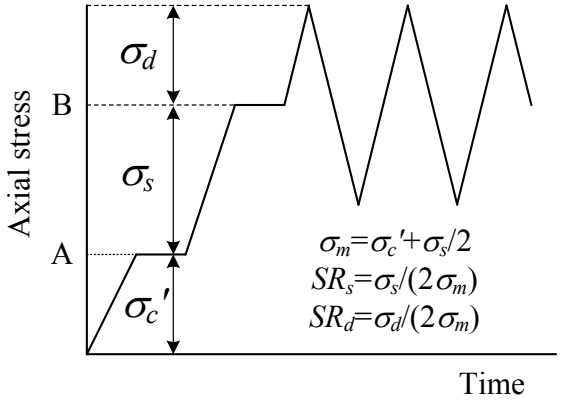

Figure 11 Definition of stress used in Eq. (1)

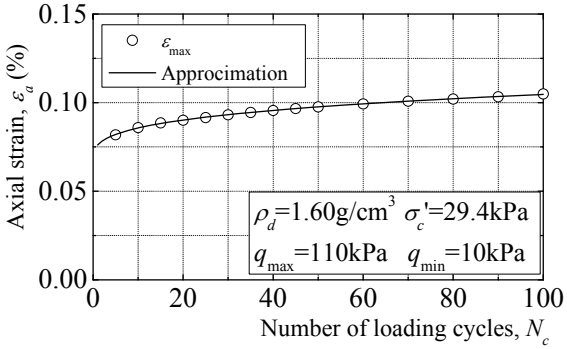

Figure 12 Estimation of cumulative axial strain

The result of a regression analysis against $(\varepsilon_a)_{max}$ - N_c relationship with Eq. (1) is shown by the solid line in Figure 12. The figure shows that the approximation adequately corresponds with the test data, thereby confirming that Eq. (1) is effective in expressing the cumulative strain characteristics of ballast. On the basis of the cumulative strain characteristics of ballast obtained from Eq. (1), the $(\varepsilon_a)_{max}$ - N_c relationships for various values of SR_s and SR_d are plotted in Figure 13. From this figure, the following findings can be drawn with regard to the cumulative strain characteristics of ballast:

- When SR_s and SR_d are constant, $(\varepsilon_a)_{max}$ increases as N_c increases.
- When SR_s and N_c are constant, $(\varepsilon_a)_{max}$ increases as SR_d increases.
- When SR_d and N_c are constant, $(\varepsilon_a)_{max}$ decreases as SR_s increases.

We assume that the empirical formula (Eq. (1)) derived from the above-mentioned regression analysis can be applied to other stress conditions examined. Besides, this study calls a theory to estimate the elasto-plastic deformation of earth structures under cyclic loading by reducing the deformation modulus in consideration of the cumulative strain characteristics of geomaterials "Cumulative damage theory." However, due to insufficient experimental results, there is room for further investigation on the validity and applicability of the empirical formula or cumulative damage theory to various loading conditions, boundary conditions and material properties in terms of the improvement of experimental reliability.

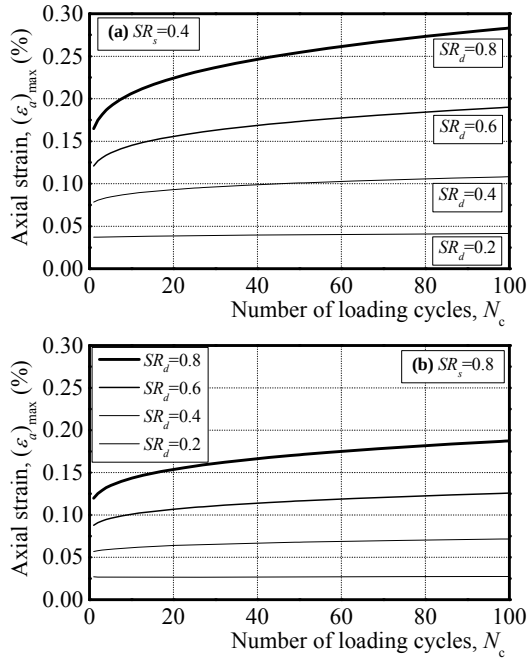

Figure 13 Cumulative strain characteristics of ballast (a: SR_s=0.4, b: SR_s=0.8)

3.2 FE analysis based on cumulative damage theory

3.2.1 Analytical procedure

As required by the "Design standard for Railway Structures - Seismic Design –", an analytical model is used for calculating the plastic deformation of earth structures like an embankment caused by the Level 2 seismic motion. In this study, the elasto-plastic deformation of ballasted track under seismic motions is estimated by the linear FE analysis with a damaged model in which the deformation modulus of FE elements representing railroad ballast has been reduced in consideration of the cumulative strain characteristics of ballast as shown in Figure 13. The outline of the proposed FE analysis based on the cumulative damage theory is provided in Figure 14. Note that for other structural members like concrete sleeper and steel roadbed which do not remarkably show the plastic deformation under cyclic loading in contrast to railroad ballast, the deformation modulus assumes to be undamaged and unchanged. The analytical procedure of setting the deformation modulus of railroad ballast and calculating the elasto-plastic deformation of ballasted track by the proposed FE analysis is as follows (Figure 14):

1. The initial stability analysis is statically conducted by applying the force of gravity to an undamaged FE model which has not experienced any seismic motions in order to calculate the initial stress (σ_s, σ_m) at each ballast element and the initial displacement (u_i) by its self-weight (Step 1 in Figure 14). For this purpose, the undamaged deformation modulus is defined by an initial tangential deformation modulus (E_0) at an extremely small strain level ($\varepsilon_a \approx 0.001\%$) obtained from triaxial compression tests on ballast (Figure 15).
2. A single seismic wave of the design seismic motion together with the force of gravity is applied to the undamaged FE model in order to conduct the dynamic response analysis, and calculate σ_d and elastic displacement (u_e) at each ballast element (Step 2 in Figure 14).
3. The σ_s, σ_d, and σ_m obtained in steps 1 and 2, and N_c are substituted into Eq. (1) to calculate the cumulative axial strain ($(\varepsilon_a)_{max}$) of each element representing railroad ballast for N_cth cyclic loading and nth convergent calculation. Then, the damaged deformation modulus ($E_{Nc}(n)$) due to the single seismic wave of the design seismic motion for each element of railroad ballast is calculated using Eq. (2) (Step 3 in Figure 14).

$$E_{Nc}(n) = \sigma_d / (\varepsilon_a)_{max} \quad (2)$$

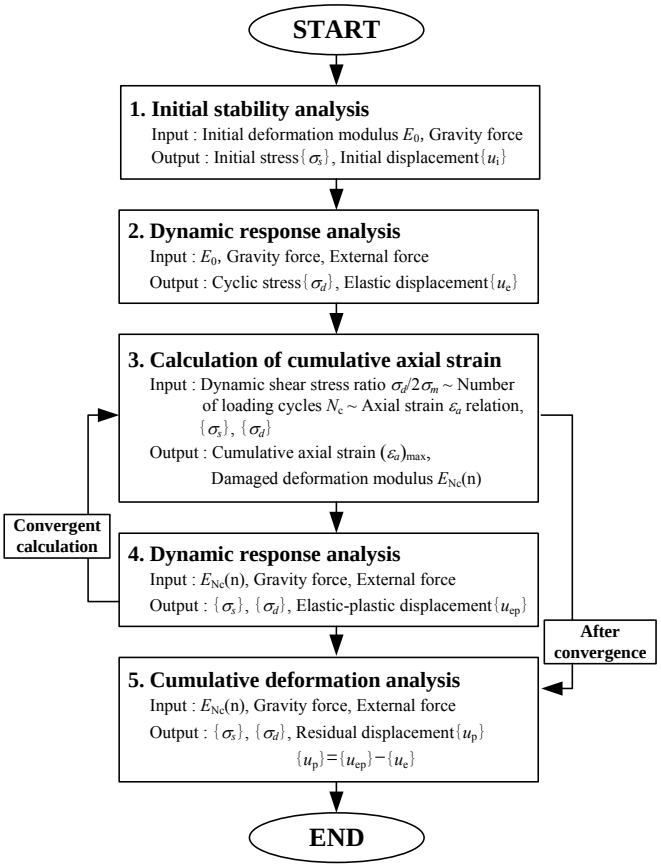

Figure 14 Proposed analytical procedure

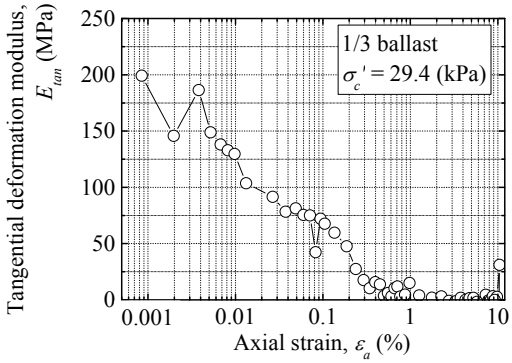

Figure 15 Tangential deformation modulus obtained from triaxial compression tests on ballast

4. Initial stability analysis and dynamic response analysis are conducted by using the calculated $E_{Nc}(n)$ in order to estimate the stress distribution (σ_s, σ_d, and σ_m) and elasto-plastic displacement (u_{ep}). Then, $(\varepsilon_a)_{max}$ and $E_{Nc}(n+1)$ for each element of railroad ballast at N_cth cyclic loading and (n+1)th convergent calculation are calculated with Eq. (1) and (2). When comparing the damaged deformation moduli obtained before and after the analysis, in case they do not agree, steps 3 and 4 are repeated until the values converge (Step 4 in Figure 14).
5. Cumulative deformation analysis is conducted by applying a single seismic wave of the design seismic motion together with the force of gravity to the damaged FE model after convergence in order to calculate u_{ep}. Then, the difference between u_{ep} and u_e is considered as the residual displacement after a seismic motion (u_p) (Step 5 in Figure 14).

For reference, some examples for the convergence of the damaged deformation modulus in step 4 are shown as in Figure 16.

The values were taken from the analytical results obtained in Section 4.2. The damaged deformation modulus gradually converges to a constant value with the convergence calculation. In this study, we consider that the damaged deformation modulus of each ballast element has converged when the rate of the deformation modulus before and after the convergence calculation became less than or equal to ±5%. Besides, at that time, we assume that each ballast element satisfies the cumulative strain characteristic under the stress condition.

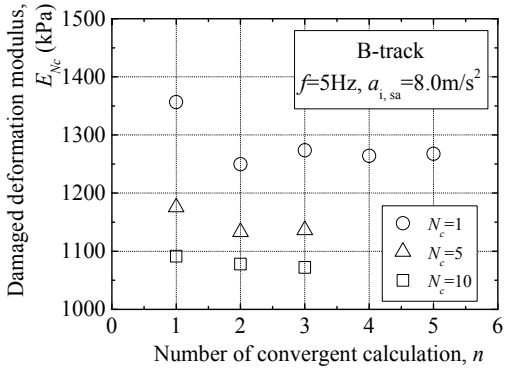

Figure 16 Convergence of damaged deformation modulus

3.2.2 Application to actual problems

For the application of the above-mentioned procedure, accordingly, it is necessary to determine σ_s, σ_d, and σ_m by using the stress at each ballast element obtained from the just past FE analysis. However, unlike the stress condition in triaxial compression tests where lateral pressure is constant when axial pressure is applied, if axial pressure is applied from one direction, the stresses of an element within soil ground for the other two directions orthogonal to it will also alter, in addition to a change in the stress for the applied direction. Accordingly, it becomes necessary to approximate the stress condition during isotropic consolidation and the stress condition during shear by using the stresses derived from the initial stability analysis and the dynamic response analysis. In this study, the approximation was made by using Eq. (3). Here, the relationships between the stresses in the triaxial compression test (σ_s, σ_d, σ_m, and σ_c') and the maximum and minimum principal stresses (σ_1 and σ_3) of an element within soil ground are shown in Figure 17.

$$\left.\begin{array}{ll} \sigma_s = \sigma_1^s - \sigma_3^s & \sigma_d = (\sigma_1^{sp} - \sigma_3^{sp}) - \sigma_s \\ \sigma_c^{'} = \sigma_3^s & \sigma_m = (\sigma_1^s + \sigma_3^s)/2 \end{array}\right\} \quad (3)$$

Where σ_1^{sp} : maximum principal stress under the force of gravity and seismic load, σ_3^{sp} : minimum principal stress under the force of gravity and seismic load, σ_1^s : maximum principal stress under the force of gravity, σ_3^s : minimum principal stress under the force of gravity.

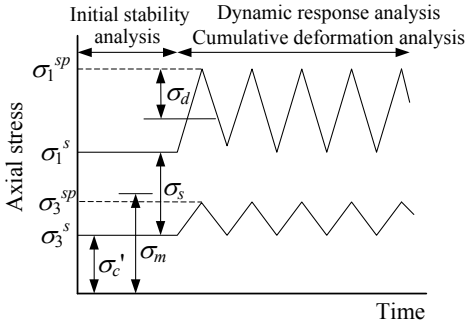

Figure 17 Relationship between principal stress and stress used in cumulative damage model

Furthermore, the maximum and minimum principal stresses generated in the soil ground as a result of seismic motion vary with time, because seismic waves are characterized by random vibrations. Thus, the loading conditions (σ_s, σ_d, σ_m, and N_c) in the soil ground under seismic motions would be different from those of the cyclic triaxial compression test with a constant stress amplitude. Therefore, when determining the loading conditions based on the time history of the dynamic shear stress ratio (SR_d) as shown in Figure 18, we consider the maximum dynamic shear stress ratio between the points of time when the input acceleration reaches zero (indicated by circles in Figure 18) as the stress amplitude of the time span; further, the number of the maximum dynamic shear stress ratio as N_c.

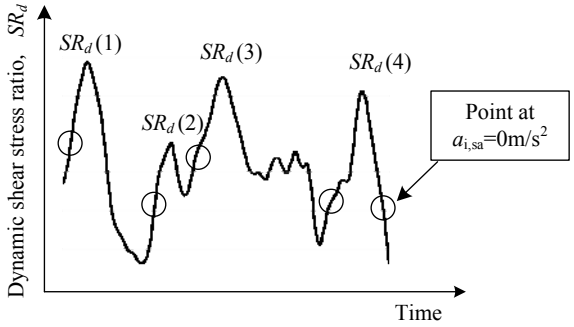

Figure 18 Time history of dynamic shear stress ratio during seismic motion

On the other hand, in the triaxial compression test for example, the loading direction of the axial pressure and that of the maximum principal stress are in agreement, however in the soil ground, the direction of the gravity or surcharge and that of the maximum principal stress are not always in agreement. For this reason, it is necessary to theoretically determine the direction of damage even when using the cumulative damage theory, because, in reality, the deterioration is not limited to the rigidity whose direction is parallel to the loading direction. However, to simplify the calculation in this study, we assume the isotropy and uniformity of material characteristics without taking into account the directionality of damage generated inside the ballast element.

4. SEISMIC RESPONSE ANALYSIS ON MODEL TRACKS UNDER HORIZONTAL VIBRATION

4.1 Analytical methods

4.1.1 Analytical model

In this section, the applicability of the analytical procedure proposed in the former section to the seismic response analysis of ballasted track structures under horizontal vibrations is reviewed by comparing the distribution of the damaged deformation moduli inside railroad ballast and the residual displacement of ballast elements obtained from the FE analysis based on the cumulative damage theory with their corresponding values obtained from the shaking table tests in Chapter 2.

An outline of the two-dimensional FE models under plane-strain condition employed for numerical simulations of shaking table tests on 1/3 small model ballasted track structures is shown in Figure 19. For the boundary conditions of the FE models, the roadbed base was completely fixed and the two sides adopt vertically sliding boundary (fixed only in the horizontal direction) in the initial stability analysis, while in the dynamic response analysis and cumulative deformation analysis the base was completely fixed and the two sides adopt horizontally sliding boundary (fixed only in the vertical direction). In addition, the mesh size of ballast elements is almost equal to the average grain size (D_{50}) of 1/3 ballast (Figure 2), because the cumulative strain characteristics of the ballast obtained from the cyclic triaxial compression tests correspond to the average behavior of the 1/3 ballast sample. In this study, we used linear FE analysis for both static and dynamic analyses.

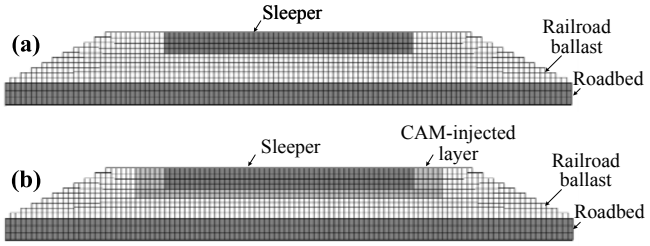

Figure 19 Numerical simulation models of shaking table tests (a: conventional ballasted track, b: grouted ballasted track)

4.1.2 Analytical conditions

The numerical simulation was conducted in three stages: initial stability analysis, dynamic response analysis, and cumulative deformation analysis, as shown in Figure 14. Gravity of 1G (9.8 m/s^2) was applied in the initial stability analysis, and a sine wave in the horizontal direction was inputted to the roadbed to simulate the design seismic motion in the dynamic response analysis and cumulative deformation analysis. The loading frequency (f) of the sine wave was 5 Hz, and the input single amplitude of base acceleration ($a_{i,sa}$) was varied from 2.0 m/s^2 to 10.0 m/s^2 in increments of 2.0 m/s^2, in the same way as the vibration conditions in the shaking table test.

The analytical input parameters used in linear FE analysis are shown in Table 2. As for railroad ballast, the initial tangential deformation modulus (E_0) was set with reference to the results of the monotonic loading triaxial compression test (Figure 15), while the damaged deformation modulus (E_{Nc}(n)) was set according to the above-mentioned analytical procedure utilizing the FE analysis based on the cumulative damage theory. Furthermore, since Tanaka et al. (1987) reported that the damping ratio for sand and gravel obtained from the cyclic triaxial compression tests are related to the ratio between the initial deformation modulus and the deformation modulus after cyclic loading, the damping ratio of railroad ballast was set at 0.2 on the basis of the range of the ratio between the undamaged and damaged deformation moduli (E_1/E_0). Moreover, the density (ρ) and Poisson ratio (ν) were set with reference to the results of cyclic triaxial compression tests on 1/3 ballast (Kohata et al., 2003) which test conditions were similar to those for the shaking table tests.

As for sleeper and roadbed, the material constants (ρ, E, and ν) were represented by common design values as shown in the design standard for railway structures in consideration of the experimental conditions of model ballasted tracks where the sleeper and the roadbed were made of concrete and steel, respectively. Besides, the material constants for the CAM-injected layer were set with reference to the results of the unconfined compression test (Figure 4). As shown above, in employing the cumulative damage theory, all the material constants, except the deformation modulus of railroad ballast, were kept constant throughout the analysis.

4.2 Results and discussions

4.2.1 Distribution of damaged deformation modulus

This section examines the damage of railroad ballast caused by horizontal vibrations. Figure 20 shows contour maps on the distribution of the ratio between the undamaged and damaged deformation moduli (E_1/E_0) for B-track at different input single amplitudes of base acceleration ($a_{i,sa}$). Similarly, Figure 21 shows the contour maps for G-track. Note that the blank rectangular section in the middle of the figures indicates the sleeper and the CAM-injected layer in which there is no decrease in the deformation modulus due to cyclic loading. Furthermore, Figure 22 compares the E_1/E_0 values for different $a_{i,sa}$ at various positions along the left end slope of railroad ballast (positions LU, LM, and LL in Figure 3) in each model track.

From the figures, it is observed that the decrease in the deformation modulus of railroad ballast due to the seismic motion increases with an increase in $a_{i,sa}$. Besides, the seismic motion caused a significant reduction in the deformation modulus at the edges of railroad ballast such as the ballast shoulders and slopes, while the reduction is relatively smaller at the center of railroad ballast, directly below the sleeper. A possible reason for this is that the confining pressure is smaller near the ballast shoulders and slopes and higher at the center directly below the sleeper. Although a similar tendency can be observed for G-track, the overall decrease in the deformation modulus of G-track is smaller than that of B-track when compared under the same loading conditions. This seems to be related to the assumption that the CAM-injected layer has a constant deformation modulus and is not damaged throughout the FE analysis. In addition, it is inferred that the estimation of the damage inside railroad ballast based on the cumulative damage theory is valid, because the above-mentioned tendencies are qualitatively in good agreement with the results of shaking table tests discussed in the former chapter.

4.2.2 Calculation method for residual displacement

This section examines how to apply the cumulative damage theory under cyclic loading. According to the analytical procedure given in Figure 14, the possible calculation methods for residual displacement under cyclic design seismic motions equivalent to 10 sine waves applied in the shaking table test on the model tracks as described in Chapter 2 are as follows. Here, Figure 23 explains the concepts for determining the damaged deformation modulus by the two methods:

(a) Assume the residual displacement ($u_{p,1}$) for a single sine wave calculated with the damaged deformation modulus (E_1) at N_c=1 constant regardless of the number of loading cycles, and regard 10 times $u_{p,1}$ as the residual displacement ($u_{p,10}$) for 10 sine waves (hereafter, "Method A").
(b) Estimate the residual displacement ($u_{p,10}$) for 10 sine waves calculated with the damaged deformation modulus (E_{10}) at N_c=10 (hereafter, "Method B")
(c) Average $u_{p,10}$ obtained from Method A and $u_{p,10}$ obtained from Method B (hereafter, "Method C")

Figure 24 compares the residual displacement at the positions LU, LM, and LL (Figure 3) in B-track obtained from the FE analyses with different calculation methods for residual displacement under the same loading condition (f=5Hz, $a_{i,sa}$ =8.0m/s^2) to experimental results reported at Paragraph 2.2.3 (Figure 10a). The residual displacement calculated by all methods increases with the vertical position, and the increasing tendency of the residual displacement calculated with every FE analysis is in agreement with that of the experimental result. When compared to the residual displacement at the same position, the residual displacement calculated by the method A is larger than experimental result irrespective of the position, whereas that calculated by the method B is smaller, and that calculated by the method C is relatively favourable. A reason for this is that the cumulative strain characteristics obtained from the cyclic triaxial compression test does not take into account the tendency for the plastic deformation of railroad ballast under horizontal vibration. In general, the density of the railroad ballast tends to decrease with the failure of the compacted ballast under cyclic loading in a shaking table test. However, the density increases with an increase in the number of loading cycles in a cyclic triaxial compression test. Accordingly, there is a possibility for the residual displacement calculated by the method B to be underestimated. In addition, the experimental results in shaking table tests show that the increase in the residual displacement decreases with cyclic loading. It is therefore possible that the residual displacement calculated by the method A was overestimated when compared to the test results. For these reasons, in this study, we adopt the method C.

Table 2 Material properties of FE model

Name	Unit mass ρ	Deformation modulus E	Poisson's ratio v
Sleeper	2.35 g/cm^3	30.0 GPa	0.20
Railroad ballast	1.60 g/cm^3	0.195 GPa*	0.49
CAM-injected layer	2.25 g/cm^3	0.405 GPa	0.30
Roadbed	7.85 g/cm^3	210.0 GPa	0.30

* : initial tangential deformation modulus (E_0)

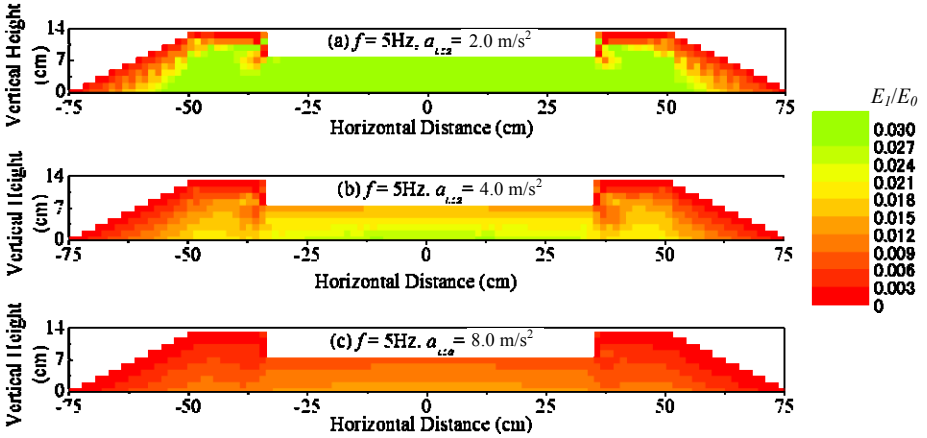

Figure 20 Distribution of ratio between undamaged and damaged deformation moduli (E_1/E_0) in conventional ballasted track

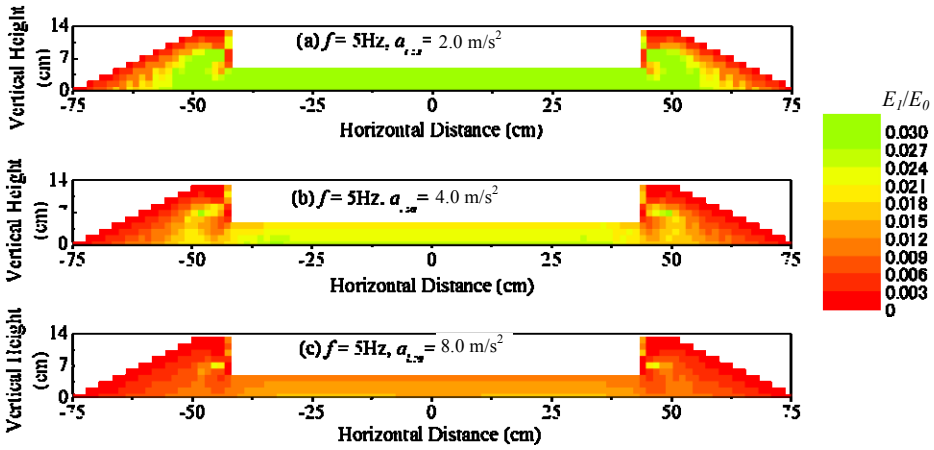

Figure 21 Distribution of ratio between undamaged and damaged deformation moduli (E_1/E_0) in grouted ballasted track

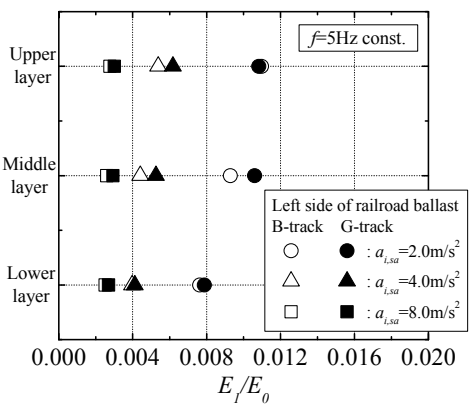

Figure 22 Influence of experimental conditions on E_1/E_0

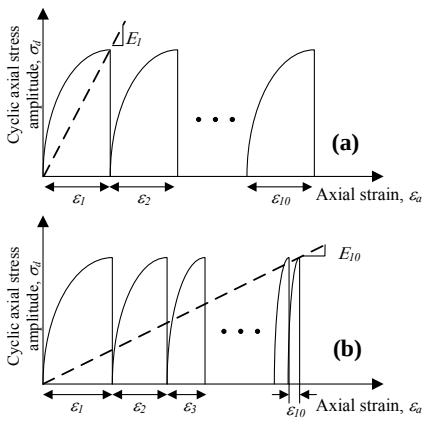

Figure 23 Cumulative damage models (a: Method A, b: Method B)

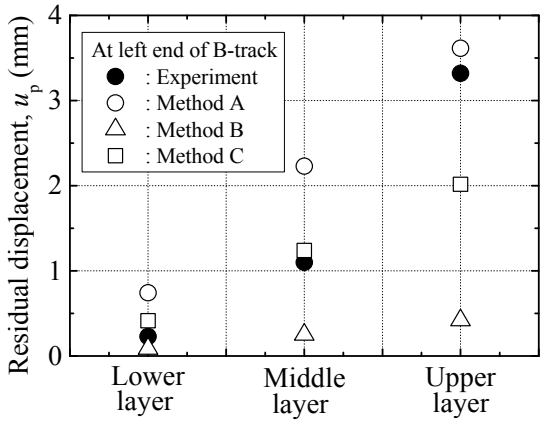

Figure 24 Influence of calculation method on residual displacement

4.2.3 Influence of input acceleration on residual displacement

This section examines the plastic deformation behavior of railroad ballast under horizontal vibration. Figure 25 compares the relationships obtained from shaking table tests and the FE analyses under the same vibration conditions between the residual displacement (u_p) and the input single amplitude of base acceleration ($a_{i,sa}$) at the positions LU, LM, and LL (Figure 3) in B-track and G-track, respectively. The residual displacement obtained from the FE analysis increases with an increase in $a_{i,sa}$, regardless of the track structure. Its increasing tendency varies with the vertical position, and the rate of increase in u_p becomes higher in the upper layer of railroad ballast. Furthermore, for the plots under the same $a_{i,sa}$, u_p for G-track is smaller than that for B-track, regardless of the vertical position.

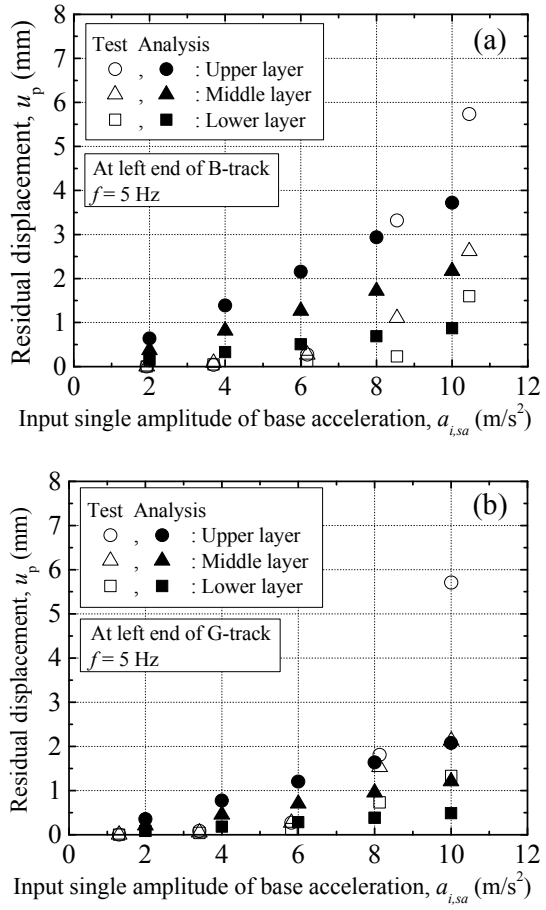

Figure 25 Comparison of u_p between test and analytical results (a: conventional ballasted track, b: grouted ballasted track)

When comparing the analytical results with the experimental results, it should be noted that the residual displacement obtained from the FE analysis is slightly higher quantitatively, although both results are qualitatively in good agreement with each other. In particular, the residual displacement obtained from the FE analysis for G-track is overestimated at the range of $a_{i,sa}$=6.0m/s^2 or less, and it is not in good agreement with the experimental results. However, on the whole, the proposed analytical procedure seems to have a sufficient analytical precision as a dynamic response analysis for ballasted track structures in case of the vibration condition over $a_{i,sa}$=6.0m/s^2. Accordingly, FE analysis based on the cumulative damage theory is expected to be capable of estimating the elasto-plastic behavior of railroad ballast to a certain extent. Especially, it is considered to be most effective for a strong seismic motion like the Level 2 seismic motion where $a_{i,sa}$ is over 6.0 m/s^2.

5. CONCLUSION

The following findings can be obtained from the present study:

1. As the dynamic behavior of ballasted track structures subjected to seismic motions has high correlation to the local plastic flow of railroad ballast caused by a large movement of constituent particles, the evaluation of the seismic stability and ductility needs to estimate the mobility of individual ballast particles under vibrations.
2. In case of the seismic design of ballasted track structures against Level 2 seismic motion, the grouted ballasted track exhibits higher aseismic performance than the conventional ballasted track because the former can restrain the damage of railroad ballast caused by seismic motions than the latter.
3. The edges of railroad ballast and the adjacent area such as ballast shoulder and slope face are prone to damages due to seismic motions and exhibit the weakest aseismic performance among various components of ballasted track structures.
4. For making use of the laboratory element tests on coarse granular materials in the prediction of the deformation behavior of railroad ballast under seismic motion, the cumulative damage theory on the basis of the cumulative strain characteristics of ballast obtained from the cyclic triaxial compression test was proposed.
5. An analytical procedure utilizing the FE analysis based on the cumulative damage theory was developed in order to estimate the residual displacement generated in ballasted track structures after an earthquake.
6. According to the comparison between experimental results of shaking table tests of small-scale model ballasted tracks and the numerical simulations, the analytical procedure could roughly estimate the residual displacement of railroad ballast after seismic motions.
7. From the viewpoints of the distribution of damaged deformation modulus and residual displacement inside railroad ballast after seismic motion, the grouted ballasted track has an advantage in the aseismic performance over the conventional ballasted track.

This study proposed a simple and practical seismic calculation method, which utilizes the FE analysis taking into consideration the cumulative strain characteristics of ballast, for evaluating the aseismic performance of ballasted track structures under Level 2 seismic motion. The foregoing findings confirm sufficient applicability of the proposed analytical procedure to the estimation of the dynamic response of ballasted track structures subjected to strong horizontal vibrations. Therefore, we expect that the outcomes of this study will be useful in developing a systematic and rational seismic design method for ballasted track structures against strong seismic motions. However, for practical application to the seismic design procedure for actual track structures, there is room for further investigation on the validity and applicability of the cumulative damage theory and the analytical procedure in terms of the improvement of experimental reliability and analytical precision.

6. REFERENCES

Hirano, K., Jiang, G.L., Tateyama, M., Chikuma, S. and Tatsuoka, F., (1997) "Deformation and cumulative strain characteristics of sandy filling material". Procs. of the 52th annual conference of the Japan Society of Civil Engineers, pp146-147. (in Japanese).

Horii, K., Tateyama, M., Kojima, K. and Koseki, J., (1997) "Earthquake induced permanent settlement of sandy embankment". Procs. of the 52th annual conference of the Japan Society of Civil Engineers, pp148-149. (in Japanese).

Ishikawa, T., and Sekine, E., (2003) "Dynamic behavior of railroad ballast in shaking table tests", Proceedings of Int. Symposium on Deformation Characteristics of Geomaterials, Lyon, pp841-848.

Kohata, Y., Miura, K., Iguchi, M. and Sekine, E., (2003) "The strength and deformation properties of the single-grained crushed stones on the similar grain size distribution". Procs. of railway mechanics, No.7, pp25-30. (in Japanese).

Miura, S. (1996) "Deformation of track and the safety of train in earthquake". QR of RTRI, 37(3), pp139-146.

Miura, S. and Kirishiki, K. (1982) "Literature search on the damage of train and track structures caused by earthquake". RTRI Pre-Report, No.82-45. (in Japanese).

Railway Technical Research Institute (1999) Design standard for Railway Structures - Seismic Design -. Tokyo: Maruzen (in Japanese).

Suda, M., Nagato, A., Tokuoka, K. and Miura, S., (1997) New railway track. Japanese Railway Civil Engineering Association. (in Japanese).

Sunaga, M., Ishikawa, T. and Namura, A., (1995) "The present designing and maintenance of railroad ballast in ballasted track". Soil mechanics and foundation engineering, 43(2), pp10-14. (in Japanese).

Tanaka, Y., Kudo, Y., Yoshida, Y. and Ikemi, M., (1987) "A study on the mechanical properties of sandy gravel - Dynamic properties of reconstituted sample -". CRIEPI Research Report, U87019. (in Japanese).